RSC Advances

PAPER

View Article Online
View Journal | View Issue

Cite this: *RSC Adv.*, 2024, **14**, 12624

Research on preparation and related properties of macro–micro porous mullite ceramic skeletons *via* twice pore-forming technology

Chunxia Xu,[ab] Rui Hu,[b] Ying Liu, *[a] Zhe Chen,[b] Zhen Liu[b] and Wenbin Han[b]

A lot of solid waste coal gangue is produced every year in the process of coal mining and coal washing, which poses a great threat to human health. How to deal with coal gangue properly is still a serious problem. In this study the macro–micro composite porous mullite ceramic skeletons were successfully prepared using solid waste coal gangue and α-Al_2O_3 as main raw materials *via* twice pore-forming technology. The main phase composition of the porous ceramic skeletons was mullite tested by X-ray Diffractometer (XRD). The morphology and microstructure of the porous ceramic skeletons were analyzed by Scanning Electron Microscope (SEM). The results show that the microstructure of porous ceramic skeletons was mainly composed of mullite whiskers. With the increase of sintering temperature from 1200 °C to 1350 °C, the maximum length of mullite whiskers grew up from 2.68 μm to 8.10 μm and their average length grew up from 0.78 μm to 2.98 μm. The maximum compressive strength of the porous ceramic skeletons with 30 PPI and 45 PPI were 1.25 MPa and 1.54 MPa tested by Universal Testing Machine (UTM) at the sintering temperature of 1250 °C, respectively. The linear shrinkage, bulk density and pore stem density of the porous ceramic skeletons became larger with the rising of sintering temperatures from 1150 °C to 1350 °C. However, the corresponding performance values of 45 PPI porous ceramic skeletons were greater than that of 30 PPI at the same sintering temperature. The prepared porous ceramic skeletons will be used in ceramic–metal wear-resistant composites for the later research and the study provides a new idea for coal gangue on the comprehensive utilization with high added value and brings both good environmental and economic benefits.

Received 19th February 2024
Accepted 8th April 2024

DOI: 10.1039/d4ra01277a

rsc.li/rsc-advances

1. Introduction

Coal gangue is the main solid waste in the process of coal mining and coal washing. A lot of coal gangue is produced every year due to the large coal consumption in the world. China alone has stockpiled 6–7 billion tons and is still increasing at the rate of more than 300 million tons per year.[1–4] Coal gangue waste can cause serious pollution to the water resources, land, air and the ecological, which poses a great threat to human health. How to deal with coal gangue properly is still a serious problem.[5–8]

The main chemical components of coal gangue are SiO_2 (30–69.98%) and Al_2O_3 (13.72–42.40%), which also are the essential substances in preparation of mullite ceramics and can replace silicon and aluminum source as raw materials.[9–12] Recently, study on the comprehensive utilization of coal gangue with high added value has aroused the interest of many scholars, especially using coal gangue as raw materials to prepare porous ceramic materials, which is one of the important way for the efficient use of coal gangue.[13–16]

Xu H. *et al.* prepared highly porous ceramics successfully using coal gangue, coal slime and coconut palm fibers as raw materials. The effects of alumina, fiber content and sintering temperature on the mechanical properties of porous ceramics were studied.[17] Low density ceramic proppant was prepared using coal gangue and flint clay by solid state sintering method. The effect on the density of the ceramic proppant and its breakage ratio were investigated fully as a function of sintering temperature.[18] S. Shaolei *et al.* prepared porous mullite ceramics by high temperature sintering method using coal gangue as the main raw material with adding proper amount of alumina and pore-forming agent, meanwhile the effect of pore-forming agent content on the compressive strength, linear shrinkage and porosity of the porous mullite ceramics were studied.[19] Q. Lü, *et al.* fabricated porous mullite ceramic supports for filtration membrane *via* recycling coal gangue at sintering temperatures from 1100 °C to 1500 °C with corn starch as pore-forming agent meanwhile systematically studied their dynamic sintering behaviors, phase evolution, shrinkage, porosity and pore size, gas permeation flux, microstructure and mechanical properties.[20]

[a]*School of Advanced Manufacturing, Nanchang University, Nanchang 330031, China. E-mail: ncu2368@163.com*

[b]*School of Mechanical Engineering, Nanchang Institute of Technology, Nanchang 330099, China*

As shown above, most ceramics use a single method to prepare microporous or macroporous ceramics. There are few reports on the preparation of macro–micro composite porous ceramics from coal gangue. In this research, porous ceramic skeletons with macroporous and microporous were prepared using coal gangue and α-Al_2O_3 as main raw materials *via* twice pore-forming technology. The effect of sintering temperature on the properties of porous ceramic skeletons was studied, which provides a new idea for coal gangue on the comprehensive utilization with high added value.

Large-scale production of mullite ceramics using twice pore-forming technology will be able to consume a large number of coal gangue, which can solve a series of environmental problems such as air, soil and surface water pollution, and avoid some geological hazards caused by accumulation of coal gangue, then bring huge environmental benefits. Meanwhile once the porous mullite ceramics production with this technology entering industrial scale stage, other things in the sintering process should be taken into account. The first issue to consider is gas emissions. Small amount of gas may be released by raw materials and decomposition of pore-forming agent during the sintering process and may cause secondary pollution to the environment without properly handling. Then it should be considered designing corresponding gas collection devices in the future research. The collected gas can be used as raw material for the preparation of useful industrial chemicals, such as H_2CO_3 or H_2SO_4, turning the gas into useful gases, which can avoid secondary environmental pollution. Second, energy consumption should be considered. The main energy used in sintering process is electric power. Further research is needed to consider developing renewable energy devices, which can convert wind power or solar power into electric power, and meet the energy consumption during the sintering process. However, the current research is still in the laboratory stage, so the gas emissions and energy consumption can be ignored.

2. Experimental

2.1 Materials

Coal gangue powder, α-Al_2O_3, starch soluble and polyurethane sponges were used as main raw materials in the study. The detailed information of the main raw materials is shown in Table 1.

The main phases of the coal gangue are quartz, kaolin and a little muscovite as shown in Fig. 1, which were measured by X-ray diffractometer (XRD). The main chemical compositions of the coal gangue used in the study are shown in Table 2, which were tested by X-ray Fluorescence (XRF). As can be seen, the main components of coal gangue are silica and alumina, accounting for 62.31% and 20.32% respectively, which also are the main chemical elements for the synthesis of mullite.

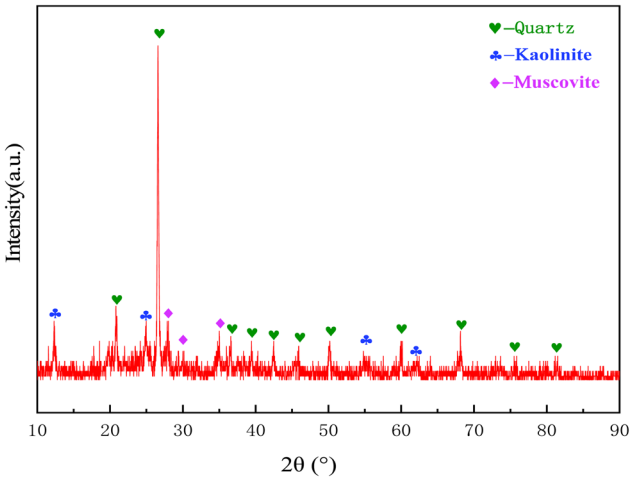

Fig. 1 XRD pattern of coal gangue.

2.2 Methods

The macro–micro porous ceramic skeletons were prepared using a novel twice pore-forming technique. The technique combines template replication and pore-forming agent method. Macropores are the first series of pores obtained by template replication. Micropores are the second series of pores obtained by the decomposition of pore-forming agents during sintering process. The macropores mainly come from copying the pores of the templates. The size of macro-pore is determined when the ceramic body is prepared with the template selected. The micropores are mainly derived from pore-forming agents, the amount of which can control the formation and size of micropores. The pore-forming agents decompose and form micropores during the sintering process. The formation and size of the macro–micro pores can be controlled by changing the pore size of the templates and the amount of pore-forming agents. After sintering, the porous ceramic skeletons with macro–micro pores can be obtained. It is an easy and well-established way to prepare porous materials with replication technique or pore-forming agent.[21–23] Most of the previous studies used a single method of template replication or pore-forming agent to prepare porous ceramics. There is few research on the preparation of ceramics *via* the twice pore-forming technique from coal gangue.

Table 1 Raw materials information

Name	Size	Corporation
Coal gangue	300 mesh	Hongyao Mineral Processing Co., Ltd, Shijiazhuang
α-Al_2O_3	1 μm	Zhongye New Materials Co., Ltd, Shanghai
Starch soluble	AR	Tianjin Zhiyuan Chemical Reagent Co., Ltd, Tianjin
Polyurethane sponges	30 PPI, 45 PPI	Yuanshengxing Electronic Material Factory, Shenzhen

Table 2 The chemical compositions of coal gangue

SiO_2	Al_2O_3	Fe_2O_3	K_2O	MgO	CaO	Na_2O	TiO_2	SO_3	P_2O_5	Others
62.31	20.32	6.83	4.08	1.83	1.45	1.20	1.15	0.240	0.144	0.446

Table 3 The main equipment used in the paper

Equipment	Type	Function
X-ray fluorescence (XRF)	ARL PERFORM'X	Chemical compositions analysis
Planetary ball Mill	QM-3SP2	Mix and grind materials
Box furnace	MXQ1200-20	Calcining coal gangue
Microwave muffle furnace	HAMiLab-C 1500	Sintering porous ceramics
X-ray diffractometer (XRD)	TD-3500	Phase analysis
Scanning electron microscope (SEM)	Quanta 200FEG03040702	Analyzing the microstructure of porous ceramics
Universal testing machine (UTM)	CSS-44100	Testing compressive strength of porous ceramics

2.3 Experimental process

The experiment process mainly included three parts: material mixing and milling, ceramic skeleton body preparation, body drying and sintering. The main equipments used in the experiment are shown in Table 3. The specific experimental steps are as follows: firstly, three raw materials are mixed (coal gangue 65 wt%, α-Al_2O_3 30 wt%, starch 5 wt%) and milled in QM-3SP2 planetary ball mill at a rotational speed of 540 rpm for 3 hours. Then proper amount of tap water is added to make ceramic slurry with 60 wt% solid mass fraction. Next, the ceramic body is prepared using polyurethane sponges as templates by dipping the ceramic slurry. After drying for 12 hours with 50 °C in drying cabinet, the ceramic bodies are sintered at different temperatures (1150–1350 °C) for 3 hours then cool to room temperature in the muffle furnace. Finally, the porous ceramic skeletons can be prepared successfully. The experimental process is shown in Fig. 2.

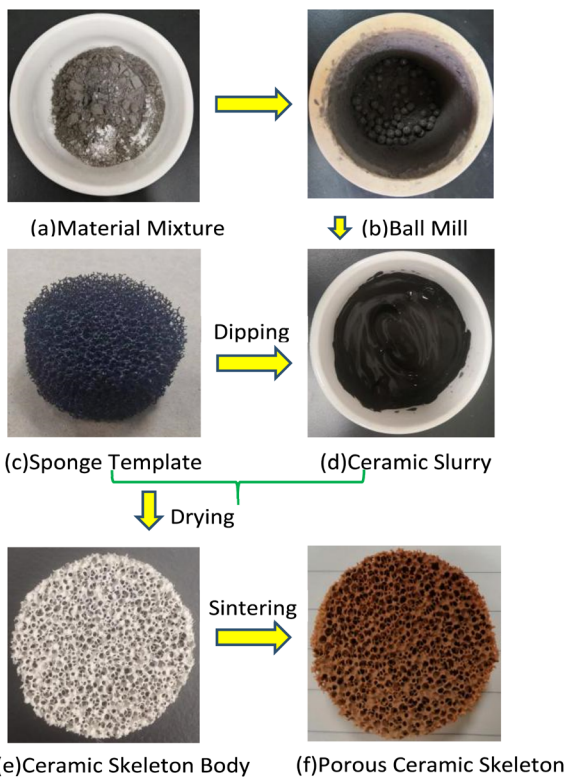

Fig. 2 The preparation process (a–f) of porous ceramic skeleton.

3. Results and discussion

The porous ceramic skeletons with 30 PPI and 45 PPI were sintered in a muffle furnace in the research. For better heating some SiC fragments were put in the saggar as absorbing materials as Fig. 3(a). To avoid collapse or crack due to excessive shrinkage stress caused by too fast heating, the porous ceramic skeleton bodies were heated slowly during the whole sintering process. The temperature curve includes three stages, the slow heating stage (I), the fast-heating stage (II) and the temperature holding stage (III).

The polyurethane sponge templates and starch decompose when the temperature is between room temperature and 650 °C. If the temperature raises too quickly, a lot of gas will be produced in a short time, which will increase the gas pressure inside the furnace, with the increase of air pressure, the ceramic skeleton body may be destroyed and even broken. So the heating rate is about 4 °C min^{-1} (stage I) before the sintering temperature reaches 650 °C and 10 °C min^{-1} (stage II) between 650 °C and the target temperature (1150–1350 °C). Then, the ceramic skeletons are kept at target temperature for 3 hours (stage III) and cool to room temperature in the furnace. Finally, the macro–micro composite porous mullite ceramic skeletons can be obtained as shown in Fig. 3(b). The sintering temperature curve is shown in Fig. 4.

3.1 Morphology characterization of the porous ceramic skeletons

The morphology characterization of the porous ceramic skeletons was gained by Scan Electron Microscope (SEM) and its

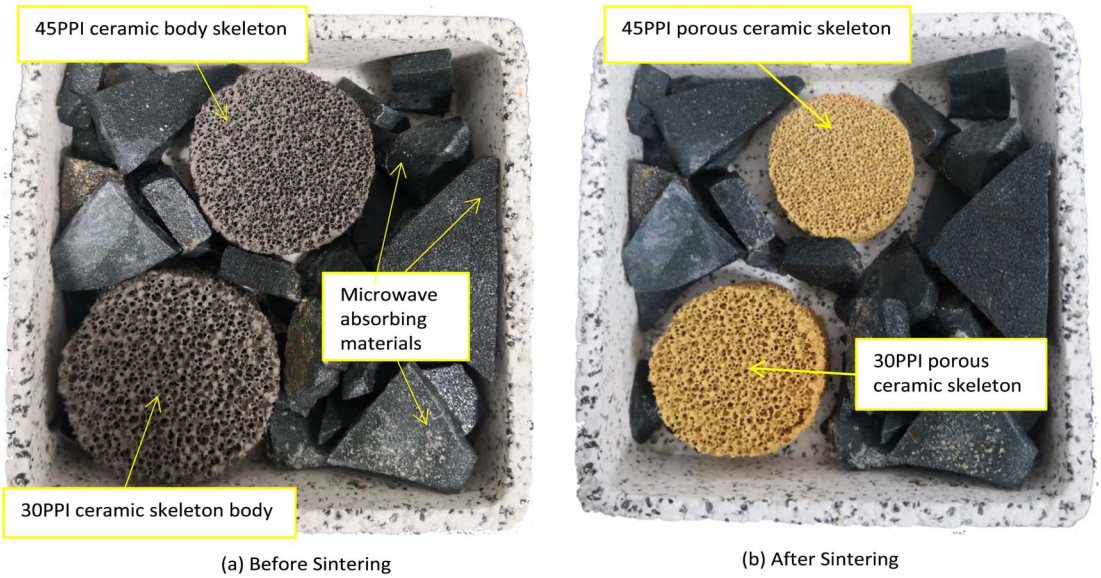

Fig. 3 Porous ceramic skeletons before sintering (a) and after sintering (b).

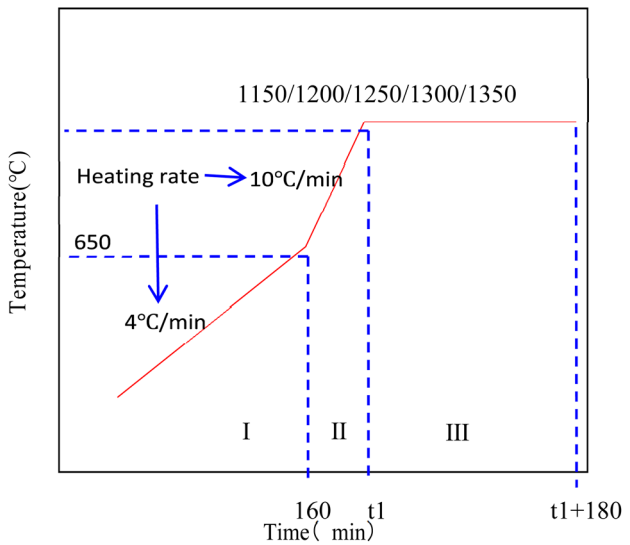

Fig. 4 Sintering temperature curve.

morphology structure consists of macro-pores and micro-pores as shown in Fig. 5(a) and (b). The macropores are obtained by replicating the pores of polyurethane sponge templates. The micropores mainly come from two sources: One kind of micropores comes from the decomposition of the polyurethane sponge templates, the other kind is from the decomposition of starch which is both binder and pore-forming agent. The macro–micro pores morphology of the porous ceramic skeletons can be seen clearly in Fig. 5(a). The pores numbered ①②④ belong to the same kind and they are mainly formed by the gas from pore stem decomposition of the polyurethane sponge templates. The pores numbered ③⑤ are mainly derived from the starch decomposition and their enlarged view is shown in Fig. 5(b). Starch additive and sintering temperature can affect the morphology of these micropores.[24,25]

3.2 Main phase of the porous ceramic skeletons

The X-ray diffractometer (XRD) was used to analyze the main phase of the porous ceramic skeletons. They should be crushed and milled into powder before testing based on the requirement of XRD for testing samples. Then the powder was placed on a test-specific slide. Finally, the sample was tested using XRD with Cu target (λ = 0.15406 nm) and the main phase of the porous ceramic skeletons was analyzed by Jade 6.0 software. The chemical equation of synthesizing mullite from silica and alumina is as following.

$$2SiO_2 + 3Al_2O_3 \rightarrow 3Al_2O_3 \cdot 2SiO_2 \quad (1)$$

Mullite synthesis temperature is relatively wide, about 1100–1600 °C. The sintering temperature of 1150 °C, 1200 °C, 1250 °C, 1300 °C, 1350 °C were chosen as the research temperature point in the study. The main phase composition of porous ceramic skeletons at different sintering temperatures are obtained as shown in Fig. 6. As can be seen from the diagram, the main phases are mullite and some corundum at 1150 °C. With the increase of sintering temperature, more and more mullite is synthesized and less alumina is left. It is very clear that most of them are mullite phase at 1350 °C. These also can be seen from some SEM images as in Fig. 7.

3.3 Microstructure of the porous ceramic skeletons

The microstructure of the porous ceramic skeletons was analyzed by SEM. In order to observe the microstructure more clearly, the porous ceramic skeletons were sprayed with the metal of gold before testing.

Fig. 7 displays the microstructure change of the porous ceramic skeletons sintered with different temperatures. The size of mullite whisker and its particle size range were measured and calculated by Nano Measurer1.2 software. The growth process of mullite whiskers can be seen clearly in the diagram.

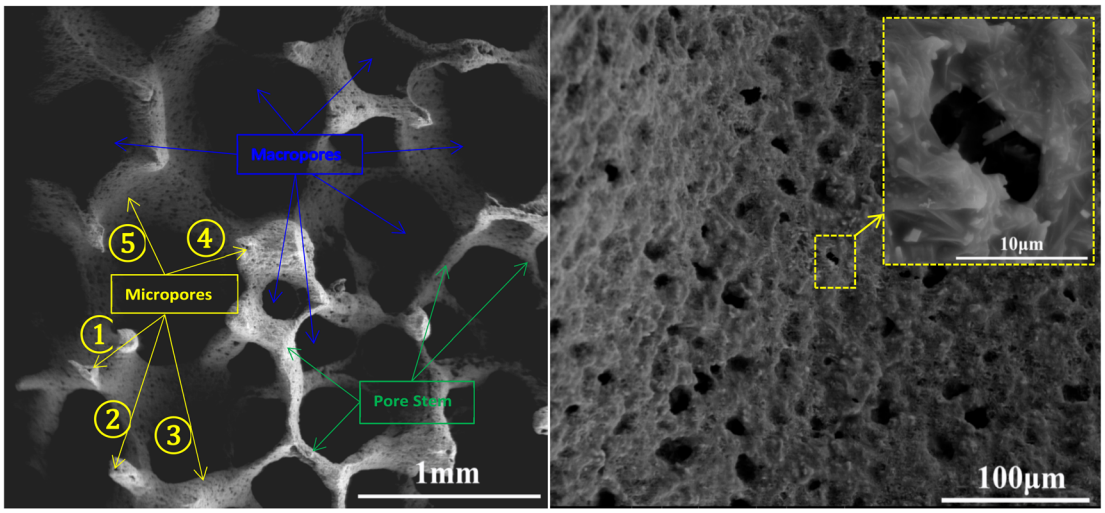

Fig. 5 The SEM morphology of the porous ceramic skeletons: (a) macro–micro composite pores and (b) magnification of micropores.

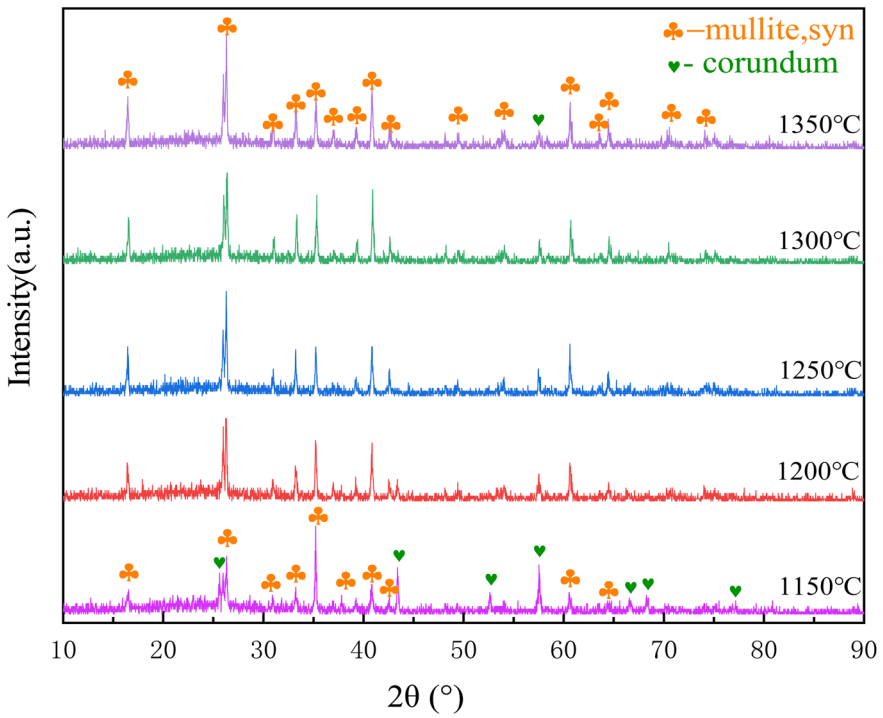

Fig. 6 XRD patterns of the ceramic skeletons observed by SEM.

Fig. 7(a) shows the microstructure of porous ceramic skeletons sintered at 1200 °C and the size of synthetic mullite is relatively small. The largest mullite whisker length is 2.68 μm and the average length of mullite whisker is 0.78 μm. In Fig. 7(b), the sintered temperature is 1250 °C. The mullite whiskers have grown a bit. Its largest length and average length are 3.96 μm and 1.56 μm respectively. In Fig. 7(c), the mullite whiskers are a little larger with sintered temperature 1300 °C than that in Fig. 7(b). Meanwhile its largest length and average length are 5.34 μm and 2.05 μm respectively. In Fig. 7(d) the ceramic skeletons were sintered at 1350 °C. The largest mullite whisker Length is 8.10 μm and its average length is 2.98 μm. More and more new mullite are formed and the crystals of synthetic mullite whiskers become larger and larger which can be seen from Fig. 7(a–d). The largest length changes from 2.68 μm, 3.96 μm, 5.34 μm to 8.10 μm and its average length changes from 0.78 μm, 1.56 μm, 2.05 μm to 2.98 μm with the increasing of sintering temperatures from 1200 °C to 1350 °C. Mullite whiskers grow up gradually as the temperature rising. The size of mullite whiskers is getting bigger and bigger which indicates that sintering temperature is one of the main factors that affects the microstructure of the porous ceramic skeletons.

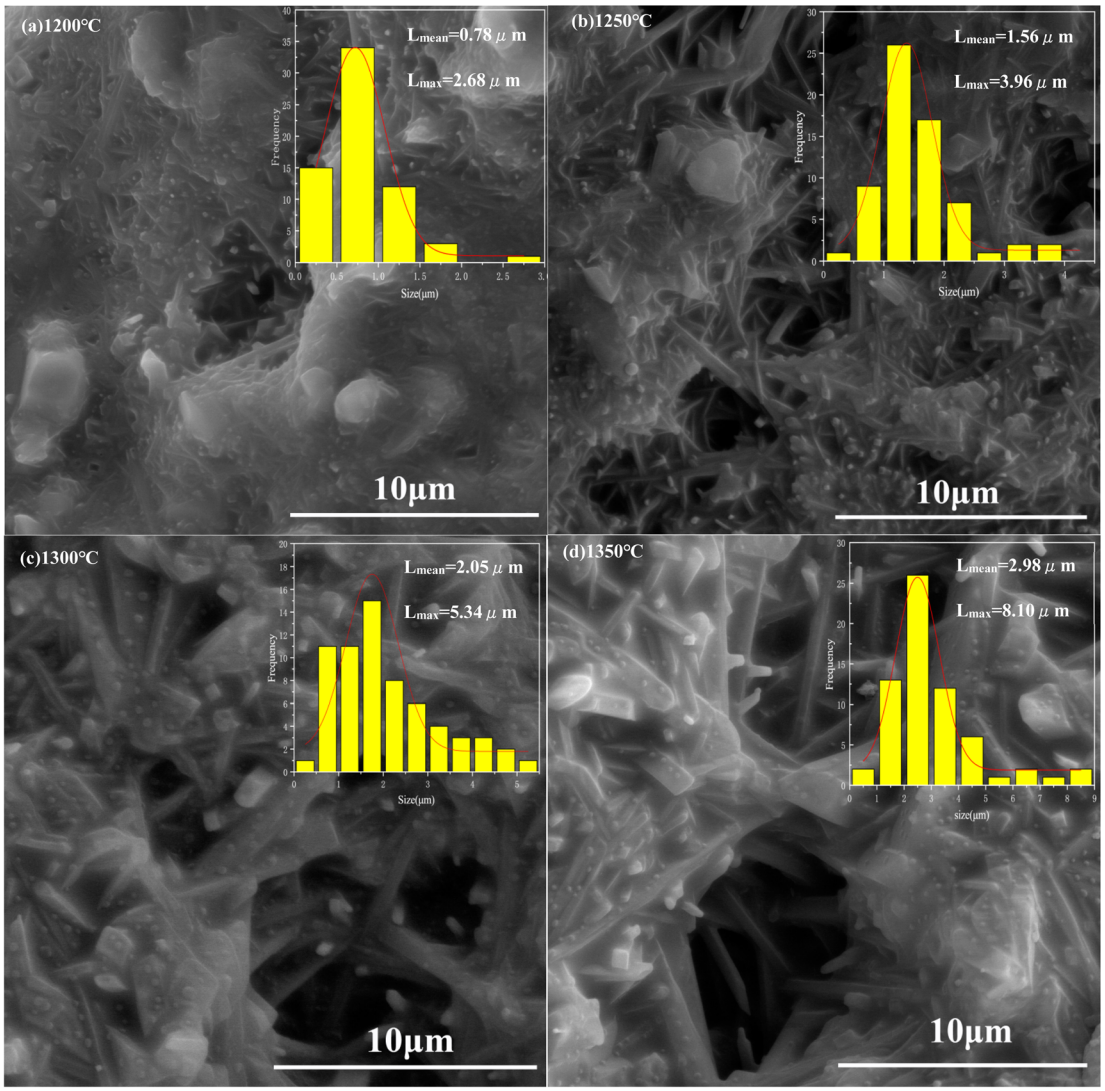

Fig. 7 The microstructure of porous ceramic skeletons: (a) 1200 °C, (b) 1250 °C, (c) 1300 °C and (d) 1350 °C.

3.4 Relevant properties of the porous mullite ceramic skeletons

Porous ceramic skeletons prepared in the paper are mainly used as the supporting skeletons of the composite material in the later research. Therefore, it focuses on the properties of linear shrinkage, bulk density, pore stem density and compressive strength. The effect of sintering temperature on these properties was studied and each temperature point data corresponds to an average value of five experiments.

3.4.1 The linear shrinkage. The ratio of linear size change to sample length during sintering is called linear shrinkage. Formula for linear shrinkage is as following eqn (2):

$$S = \frac{L_0 - L}{L_0} \times 100\% \quad (2)$$

where L_0 and L refer to the dimensions of ceramic skeleton body and sintered ceramic skeleton, respectively.[26]

Fig. 8 shows the linear shrinkage of the 30 PPI and 45 PPI porous ceramic skeletons with different sintering temperatures. With the increase of the surface energy of ceramic molecules, the interaction force between molecules increases and the binding between molecules becomes closer at high temperature, thus resulting in shrinkage. As can be seen from the diagram, the linear shrinkage of the porous ceramic skeletons with 30 PPI increases from 14.22% to 17.33%, meanwhile the linear shrinkage with 45 PPI increases from 15.93% to 18.13% as sintering temperature rising from 1150 °C to 1350 °C. The linear shrinkage rate of 45 PPI is greater than that of 30 PPI. This is because the macropores of the 45 PPI polyurethane sponge templates are relatively smaller than those of the 30 PPI, so the pore stems are denser per unit volume, which leave more shrinkage space after decomposition.

3.4.2 The bulk density. The bulk density of ceramic skeletons is the ratio of its total mass to total volume. The formula for calculating the bulk density is as following eqn (3):

$$\rho = \frac{m}{V} \quad (3)$$

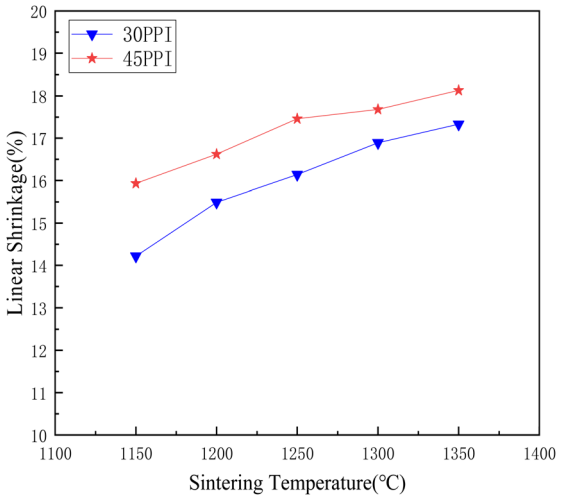

Fig. 8 Linear shrinkage with different sintering temperatures.

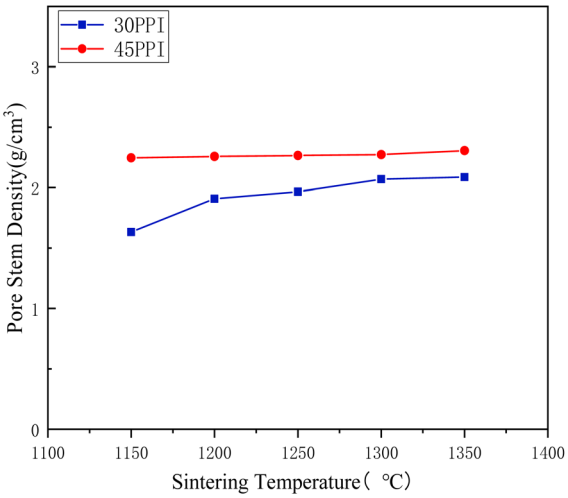

Fig. 10 Pore stem density with different temperatures.

where m and V are the mass and volume of the porous ceramic skeletons. It can be seen from the diagram that the bulk density increases with the rising of sintering temperature.[26]

Fig. 9 shows the change of bulk density with different sintering temperatures. As the sintering temperature rising from 1150 °C to 1350 °C, the bulk density of the porous ceramic skeletons with 30 PPI increases from 0.34 g cm^{-3} to 0.44 g cm^{-3}. The bulk density of the 45 PPI porous ceramic skeletons increases from 0.42 g cm^{-3} to 0.60 g cm^{-3}. The bulk density of the 45 PPI ceramic skeletons is higher than that of 30 PPI at the same sintering temperature, for the sponge templates 45 PPI have a greater pore stem density and adhere to a relatively larger amount of ceramic slurry than that of 30 PPI sponge templates, so the bulk density is relatively high.

3.4.3 The pore stem density. The pore stem density was the actual density of the solid ceramic part except open pores and it became larger if the ceramic skeleton had fewer closed pores, on the contrary the pore stem density was small. The pore stem density could be used to evaluate the number of micropores inside the ceramic. The weight of the porous ceramic skeletons could be measured by a digital balance and the volume could be gained *via* Archimedes principle, finally the pore stem density could be calculated.

Fig. 10 shows the change of the pore stem density at different sintering temperatures. As could be seen from the diagram, with the increase of temperature from 1150 °C to 1350 °C, the pore stem density of porous ceramic skeletons with 30 PPI changed from 1.63 g cm^{-3} to 2.09 g cm^{-3}. The pore stem density of the 45 PPI porous ceramic skeletons increased from 2.25 g cm^{-3} to 2.31 g cm^{-3}. The pore stem density gradually became dense with the rising of sintering temperatures. The overall pore stem density of 45 PPI was higher than that of 30 PPI. That was because the pore stem of 30 PPI sponge templates was bigger than that of 45 PPI sponge templates, which would leave bigger space after decomposing at high temperatures, so the kind of ①②④ micropores of 30 PPI (seen from Fig. 5) were much bigger than that of 45 PPI, which led to the lower pore stem density. This space was gradually being filled through shrinking with the rising of temperature. The difference of pore stem density between them decreases gradually and tends to be stable.

3.4.4 Maximum compressive strength. The compressive strength was tested by Universal Testing Machine (UTM). The citeria for judging failure is that when the test force is greater than 500 N and falls to the 50% of the peak force. The dropping speed of the UTM pressure head is 2 mm min^{-1}. The area of each sample should be calculated and input into the test system and the system automatically calculated the pressure of the sample after testing experiment, using the following eqn (4):

$$P = \frac{F}{S} \tag{4}$$

where F is the test force and S is the area of each sample. After 40 experiments, the compressive strength were obtained at sintering temperature (1150–1350 °C) with keeping the target sintering temperature for 3 hours.

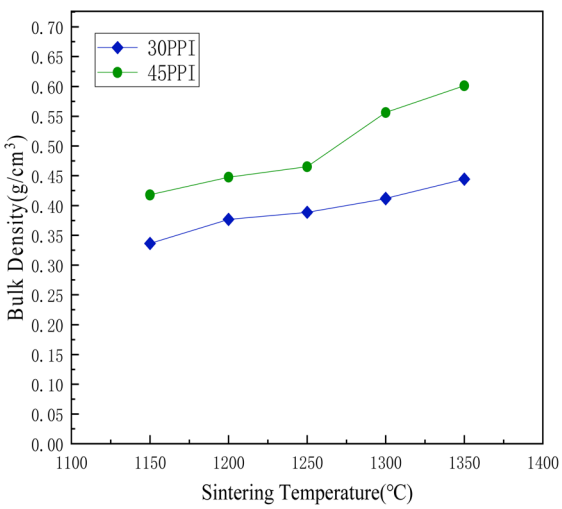

Fig. 9 Bulk density with different sintering temperatures.

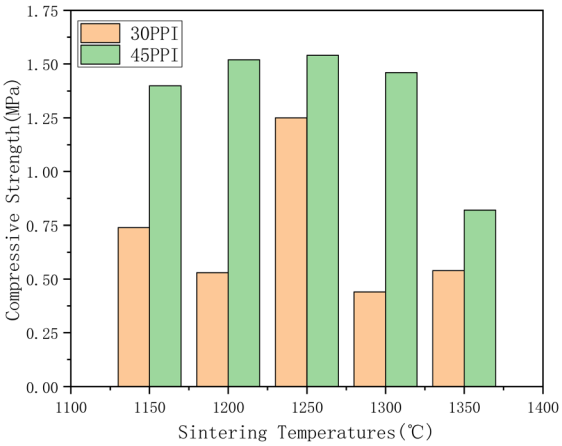

Fig. 11 The compressive strength with different sintering temperatures.

As shown in Fig. 11, the compressive strength of the ceramic skeletons are different with each other as the sintering temperature change. In general, the compressive strength with 30 PPI is lower at all sintering temperature points due to the overall macropores of 30 PPI are greater than that of 45 PPI. The synthesis reaction is not fully completed when the sintering temperature is below 1250 °C and there are some raw materials in the ceramic skeletons that are not participated in the reaction. When the sintering temperature reaches 1250 °C, most of the raw materials have been synthesized into mullite. But the mullite whiskers have not grown too big and they interlace with each other so that the ceramics have relatively good performance. When the sintering temperature is higher than 1250 °C, the mullite whiskers grow up quickly, which leads to the bigger ratio of length to diameter of the mullite whisker. It is possibly easier to be broken when the mullite whiskers become longer, so the brittleness of the ceramic skeleton increases and the compressive strength decreases. Both the ceramic skeletons with 30 PPI and 45 PPI get the maximum compressive strength value at the sintering temperature of 1250 °C, which are 1.25 Mpa and1.54 MPa, respectively.

4. Conclusions

The macro–micro porous mullite ceramic skeletons were prepared successfully *via* twice pore-forming technology, which will be used for further research of ceramic–metal wear-resistant composites. The morphology, microstructure and related properties of the porous ceramic skeletons were studied. The main research results of the paper are as follows.

(1) The morphology of the porous ceramic skeletons consists of macro-pores which were obtained by replicating the sponge template and micro-pores which were derived from the decomposition of the pore-forming agent.

(2) The main phase of porous ceramic skeletons is mullite, which was synthesized from silicon dioxide and alumina at high temperatures. More and more mullite are synthesized meanwhile the mullite whiskers grow up gradually with the rising of sintering temperature. The average length of mullite whisker increases from 0.78 μm to 2.98 μm and its maximum length increases from 2.68 μm to 8.10 μm when the sintering temperature changes from 1200 °C to 1350 °C.

(3) The related properties varies with sintering temperatures changing from 1150 °C to 1350 °C. According to the rising temperature above, the linear shrinkage of 30 PPI porous ceramic skeletons increases from 14.22% to 17.33%, and the linear shrinkage of 45 PPI porous ceramic skeletons increases from 15.93% to 18.13%; The bulk density of the porous ceramic skeletons with 30 PPI increases from 0.34 g cm^{-3} to 0.44 g cm^{-3}, however the bulk density of the 45 PPI porous ceramic skeletons increases from 0.42 g cm^{-3} to 0.6 g cm^{-3}; the pore stem density of porous ceramic skeletons with 30 PPI changes from 1.63 g cm^{-3} to 2.09 g cm^{-3}, meanwhile the pore stem density of 45 PPI porous ceramic skeletons increases from 2.25 g cm^{-3} to 2.31 g cm^{-3}. Generally speaking, the corresponding performance values of 45 PPI porous ceramic skeletons were larger than those of 30 PPI.

(4) At the sintering temperature of 1250 °C, the maximum compressive strength of porous ceramic skeletons with 30 PPI and 45 PPI are 1.25 MPa and 1.54 MPa, respectively.

Porous ceramics are widely used as filters, reactor components, electronics and building materials.[27] The macro–micro porous ceramics prepared in this study also have great potential applications in these fields and the scope of application may be more extensive, because of the unique macro–micro pore structure.

Up to now, the porous materials made from solid wastes are mainly used in absorbing and filtering materials,[28,29] however the study on wear-resistant composites is still in the primary stage. The ceramic–metal composite material will be prepared using high temperature vacuum immersion method in the later research, which have good wear resistance, tribological stability and high bearing capacity due to the unique three-dimensional structure. The macro-pores in the composite will be fully filled with metal and the micro-pores will be retained. It can be used in sliding bearings, especially in high precision aerostatic bearings. The micro-pores of the composite material can store a certain amount of lubricant and reduce the effective contact area of the friction pair, which can help the sliding bearing quickly enter the state of hydrodynamic lubrication. Also, in high precision aerostatic bearing, the micro-pores can balance the pressure inside the bearing and are helpful for the formation of lubricating gas film, which can make the bearing run stably, reduce the friction vibration and improve the precision of related equipment. The ceramic–metal composite material has great engineering application prospects in the bearing field. It is a new direction of utilization for coal gangue, which is worth of further exploration. There is still a long way to go on the preparation and application of porous ceramics from coal gangue.[30,31]

Author contributions

All authors have made important contributions to the study.

Conflicts of interest

There are no conflicts to declare.

Acknowledgements

We would like to acknowledge the National Natural Science Foundation of China (Grant No. 52365026, 51765044); Natural Science Foundation of Jiangxi Province in China (Grant No. 20212BAB204038).

References

1 W. Song, J. Zhang, M. Li, H. Yan, Y. Y. Zhou N and Y. Guo, *Appl. Sci.*, 2022, **12**, 12060.
2 Y. Hao, X. Guo, X. Yao, R. Han, L. Li and M. Zhang, *Materials*, 2022, **15**(13), 1–27.
3 L. Haibin and L. Zhenling, *Resour., Conserv. Recycl.*, 2010, **54**, 1331–1340.
4 J. Li and J. Wang, *J. Cleaner Prod.*, 2019, **239**, 117946.
5 R. Han, X. Guo, J. Guan, X. Yao and Y. Hao, *Polymers*, 2022, **14**, 3861.
6 Y. Zhang and T. C. Ling, *Constr. Build. Mater.*, 2020, **234**, 117424.
7 A. Bigeard, P. Vespa, P. Leplay, C. Mesnager, O. Citti, D. Bouvard and D. Jauffres, *J. Eur. Ceram. Soc.*, 2024, **44**(2), 1256–1266.
8 W. Liu, Y. Wang, J. Li and B. Li, *Int. J. Appl. Ceram. Technol.*, 2023, **20**(6), 3584–3595.
9 X. Li, M. Pan, M. Tao, W. Liu, Z. Gao and C. Ma, *Ceram. Int.*, 2022, **48**(24), 37055–37063.
10 X. Li, J. Shao, J. Zheng, C. Bai, X. Zhang, Y. Qiao and P. Colombo, *Int. J. Appl. Ceram. Technol.*, 2023, **20**(4), 2099–2124.
11 X. Li, M. Tao, M. Pan, W. Liu, Z. Gao, H. Yuan and C. Ma, *J. Eur. Ceram. Soc.*, 2022, **42**(13), 6015–6024.
12 Z. Liu, C. Wu, N. Xie, J. Zhu, Y. Liu, S. Huang, X. Shen, Z. Yang, X. Lin and L. Kong, *Int. J. Appl. Ceram. Technol.*, 2022, **19**(3), 1659–1668.
13 E. Gregorová, P. Šimonová and W. Pabst, *J. Eur. Ceram. Soc.*, 2024, **44**(2), 1081–1094.
14 N. M. A. A. Muhamad, L. C. Hong, Z. Arifin Ahmad and H. Md Akil, *J. Mater. Process. Technol.*, 2008, **207**(1–3), 235–239.
15 J. Du, A. Ma, X. Wang and X. Zheng, *Materials*, 2023, **16**, 5434.
16 C. Jiang, S. Huang, X. Zhang and X. Cheng, *RSC Adv.*, 2019, **9**(62), 36308–36315.
17 H. Xu, H. Du, L. Kang, Q. Cheng, D. Feng and S. Xia, *J. Renewable Mater.*, 2021, **9**(12), 2129–2140.
18 J. Hao, H. Hao, Y. Gao, X. Li, M. Qin and K. Wang, *Medziagotyra*, 2020, **26**, 94–98.
19 S. Shaolei, Z. Qiang, W. Fangfang and W. Yali, *Refractories*, 2014, **48**(1), 18–21.
20 Q. Lü, X. Dong, Z. Zhu and Y. Dong, *J. Hazard. Mater.*, 2014, **273**, 136–145.
21 K. Schwartzwalder and A. V. Somers, US Pat. No. 3090094, 1963.
22 A. R. Studart, U. T. Gonzenbach, E. Tervoort and L. J. Gauckler, *J. Am. Ceram. Soc.*, 2006, **89**(6), 1771–1789.
23 J. Pascual, J. Zapatero, M. C. Jiménez De Haro, I. Varona, A. Justo, J. L. Pérez-Rodríguez and P. J. Sánchez-Soto, *J. Mater. Chem.*, 2000, **10**(6), 1409–1414.
24 Y. Wang, S. Zhu, X. Zhou and T. Zhang, *J. Phys.: Conf. Ser.*, 2022, **2206**, 012037.
25 D. Xu, W. Li, L. Wang, W. Wang and W. D. Fei, *RSC Adv.*, 2014, **4**(64), 34008–34013.
26 M. Liu, Z. Zhu, Z. Zhang, Y. Chu, B. Yuan and Z. Wei, *Sep. Purif. Technol.*, 2020, **237**, 116483.
27 D. Haase, A. Füssel, J. Adler and U. Petasch, 60 Years of Open-Celled Ceramics Based on Replica Technique: Applications, Obstacles, and Opportunities, *Adv. Eng. Mater.*, 2024, 2301804.
28 X. Zhang, X. Chen, W. Min, G. Liang, W. Zhang, S. Yao and X. Zhong, *RSC Adv.*, 2024, **14**(2), 1009–1017.
29 G. Li, L. Mao, B. Zhu, X. Chang, Y. Wang, G. Wang, K. Zhang, Y. Tian and L. Liang, *J. Mater. Chem. C*, 2020, **8**(40), 14238–14245.
30 Y. Huang, N. Hu, Y. Ye, F. Fu, Y. Lv, J. Jia, D. Chen, Z. Ou and J. Li, *Ceram. Int.*, 2022, **48**(24), 37488–37491.
31 C. Miao, L. Liang, F. Zhang, S. Chen, K. Shang, J. Jiang, Y. Zhang and J. Ouyang, *Int. J. Miner., Metall. Mater.*, 2022, **29**(3), 424–438.